Synthetic Levers Enabling Independent Control of Phase, Size, and Morphology in Nickel Phosphide Nanoparticles

Elayaraja Muthuswamy, Galbokka H. Layan Savithra, and Stephanie L. Brock*

Department of Chemistry, Wayne State University, Detroit, Michigan 48202, United States

ABSTRACT Simultaneous control of phase, size, and morphology in nanoscale nickel phosphides is reported. Phase-pure samples of discrete nanoparticles of $Ni_{12}P_5$ and Ni_2P in hollow and solid morphologies can be prepared in a range of sizes (10−32 nm) by tuning key interdependent synthetic levers (P:Ni precursor ratio, temperature, time, oleylamine quantity). Size and morphology are controlled by the P:Ni ratio in the synthesis of the precursor particles, with large, hollow particles formed at low P:Ni and small, solid particles formed at high P:Ni. The P:Ni ratio also impacts the phase at the crystallization temperature (300−350 °C), with metal-rich $Ni_{12}P_5$ generated at low P:Ni and Ni_2P at high P:Ni. Moreover, the product phase formed can be decoupled from the initial precursor ratio by the addition of more "P" at the crystallization temperature. This enables formation of hollow particles (favored by low P:Ni) of Ni_2P (favored by high P:Ni). Increasing temperature and time also favor formation of Ni_2P, by generating more reactive P and providing sufficient time for conversion to the thermodynamic product. Finally, increasing oleylamine concentration allows $Ni_{12}P_5$ to be obtained under high P:Ni precursor ratios that favor solid particle formation. Oleylamine concentration also acts to "tune" the size of the voids in particles formed at low P:Ni ratios, enabling access to $Ni_{12}P_5$ particles with different void sizes. This approach enables an unprecedented level of control over phase and morphology of nickel phosphide nanoparticles, paving the way for systematic investigation of the impact of these parameters on hydrodesulfurization activities of nickel phosphides.

KEYWORDS: nickel phosphides · nanoparticles · phase control · morphology control

Metal-rich transition metal phosphides are a class of materials receiving considerable interest for their hydrotreating catalytic properties in the processing of fuels. Among compositions studied to date, Ni_2P is reported to be the most efficient hydrodesulfurization (HDS) catalyst, even outperforming the commercially used Ni−Mo−S/Al_2O_3 catalysts in terms of activity and resistance to poisoning.[1−3] Thus, there has been considerable interest in developing methods for synthesizing nanoscale nickel phosphides, largely focused on Ni_2P.[4−8] Many of these methods suffer from generation of competing phases and/or lack of size and morphology control, underscoring a significant need for synthetic levers that enable these characteristics to be controlled.

Synthetic methods reported for the preparation of nanoscale Ni_2P in different forms (solid particles, hollow particles, rods, and wires) include decomposition of single source precursors,[8] high temperature reduction of supported phosphates,[9,10] reaction of supported Ni and NiO particles with PH_3,[11] chemical vapor deposition,[12] solvothermal synthesis,[13] and microwave synthesis.[14] Among these, solution-based strategies that involve reaction of salts or organometallic reagents together with phosphines, or transformation of metal or metal oxide nanoparticles with phosphines, have a high potential to enable control of size and morphology in addition to phase—all relevant parameters for catalytic properties.[4−7,15,16] Our group first reported on the formation of nearly monodisperse solid spherical Ni_2P nanoparticles in the size range 7−16 nm by the reaction of bis(1,5-cyclooctadiene)-nickel(0) and trioctylphosphine (TOP) at 345 °C in trioctylphosphine oxide (TOPO).[5] The formation of hollow Ni_2P nanoparticles was first reported by Chiang and co-workers[6] and Schaak and co-workers[7] by the reaction of preformed crystalline Ni nanoparticles with TOP, followed by another report on tuning void sizes in these systems.[17] Schaak and co-workers suggested that the formation of hollow structures could be dependent on the size of the Ni nanoparticles, as smaller Ni nanoparticles (<5 nm) did not result in voids under identical transformation conditions. In very recent work, Tracy and co-workers demonstrated that the formation of hollow and solid structures depends on the ratio of P:Ni in the precursor mixture, but the final products they reported were always mixed phase (Ni_2P and $Ni_{12}P_5$).[18] To our knowledge, the ability to simultaneously control phase, size, and morphology has yet to be demonstrated for the Ni_xP_y system, or indeed any other nanoscale phosphides.

Our previous investigation on iron phosphide nanoparticles clearly indicates that

* Address correspondence to sbrock@chem.wayne.edu.

Received for review December 6, 2010 and accepted February 15, 2011.

Published online March 07, 2011
10.1021/nn1033357

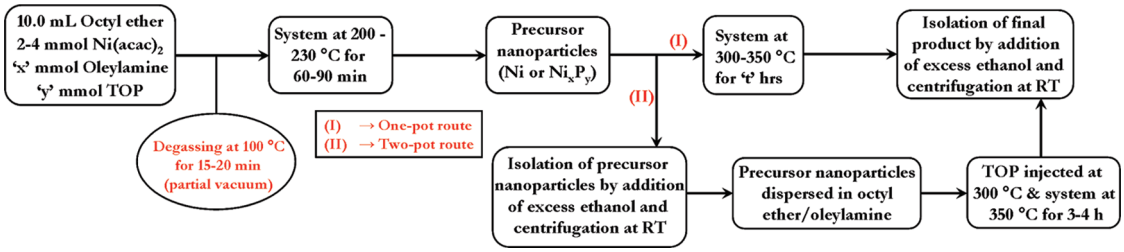

Scheme 1. Reaction pathways indicating the preparation of Ni−P nanoparticles.

the issue of phase impurity can be solved by understanding the reaction mechanism. Phase-pure samples of Fe_2P and FeP were prepared by appropriate choice of reaction conditions, arrived at by carrying out a series of reactions evaluating the effect of temperature, reaction time, Fe:P precursor ratio, and order of addition of reagents on the phase of the final product.[19] We expect that the concepts we have learned regarding phase control in the Fe−P system can be successfully extended to the Ni−P system to generate phase-pure samples and enable access to different compositions. Furthermore, a systematic study evaluating the various reaction parameters enables the factors responsible for the control of size and morphology in this system to be discerned.

Our objectives are to (i) extend the successful phase control strategy established for the Fe−P system to the Ni−P system; and (ii) uncover the factors that play a primary role in the formation of solid and hollow nanostructures in the Ni−P system. To achieve these objectives, we have adapted the general strategy originally employed by Schaak and co-workers,[7,16] and extended by others,[18] in which precursor nanoparticles containing Ni are reacted with TOP to yield nickel phosphide nanoparticles. The role of precursor ratio (P:Ni), oleylamine quantity, temperature, and heating time, in determining the phase, size, and morphology of the final product will be described and discussed in light of the reaction mechanism. Moreover, synthetic procedures enabling access to phase-pure Ni_2P and $Ni_{12}P_5$ as either hollow or solid spherical nanoparticles will be presented.

RESULTS AND DISCUSSION

Formation of nickel phosphide nanoparticles was achieved by reaction of $Ni(acac)_2$ with TOP as the P source in the presence of octyl ether and oleylamine in a two-step process involving generation of precursor particles at 200−230 °C followed by further reaction and crystallization at 300−350 °C. While the reactive form of P is not known, PH_3 generated from alkene elimination steps has been purported to be the active species in iron phosphide nanorod formation from iron nanoparticles.[20] Thus, TOP acts as both a coordinating solvent and a reactant. As shown in Scheme 1, the reactions were performed either in one pot (route I) or two pots (route II), with isolation of precursor nanoparticles occurring in the latter.

Phase Control (Ni_2P *vs* $Ni_{12}P_5$). Our previous work on the nanoscale iron phosphides clearly indicated that the choice of P:M (phosphorus/metal) precursor ratio, reaction temperature and heating time are key factors that determine the stoichiometry of the product.[19] $Ni_{12}P_5$ (tetragonal)[8,18,21,22] and Ni_2P (hexagonal)[4−7] are the most commonly observed phases in the preparation of nanoscale nickel phosphides. A series of reactions were carried out to understand the effect of heating time at different TOP:$Ni(acac)_2$ ratios and reaction temperatures (Supporting Information, Figure S1 and S2). Although the effects of P:Ni precursor ratio and temperature were not studied independently, the obtained results clearly indicate that low P:Ni ratios, lower temperatures, and shorter times favor $Ni_{12}P_5$ formation. Accordingly, a P:Ni precursor ratio of 1.12 (4 mmol $Ni(acac)_2$ and 2 mL of TOP) with 3 equiv of oleylamine (relative to Ni) and a reaction temperature of 300 °C for 1 h provided optimal conditions for generating phase-pure $Ni_{12}P_5$, as shown from the PXRD pattern in Figure 1a. Likewise, to stabilize a more P-rich phase, keeping other conditions constant, the conversion reaction was carried out for a longer time (3 h) at a higher temperature (350 °C) with an increased P:Ni precursor ratio of 5.6. When analyzed by PXRD, the product was found to be a perfect match for the more P-rich phase, Ni_2P (Figure 1b). These observations are consistent with the behavior exhibited in the Fe−P system, and highlight the successful extension of the phase control strategy we first developed for the Fe−P system to Ni−P.[19]

TEM analyses of Ni_2P nanoparticles (P:Ni = 5.6, 3 h, 350 °C,) revealed the sample to be composed of solid spherical nanoparticles (Figure 2a) with an average size of 10.2 ± 0.9 nm (Supporting Information, Figure S3a). The P:Ni atomic percent composition obtained from the EDS data was somewhat higher than the expected value for the Ni_2P phase (Figure S3b), attributed to residual TOP ligands or a reaction byproduct bound to the surface of the Ni_2P nanoparticles that was not removed in the washing step.[5] In contrast, TEM analyses of $Ni_{12}P_5$ nanoparticles (P:Ni = 1.12, 1 h, 300 °C) revealed the formation of nearly spherical hollow nanostructures (Figure 2b) of size 26.8 ± 1.9 nm (Figure S4a). EDS data

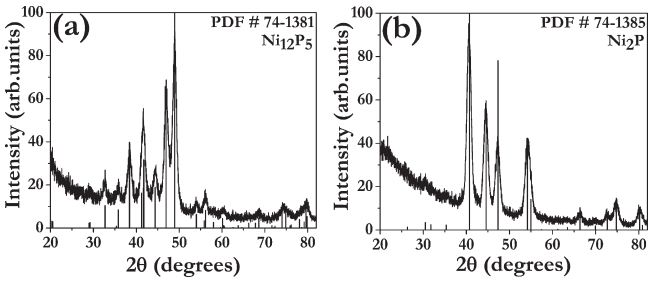

Figure 1. PXRD patterns of (a) $Ni_{12}P_5$ nanoparticles and (b) Ni_2P nanoparticles compared to line diagrams of their corresponding reference patterns.

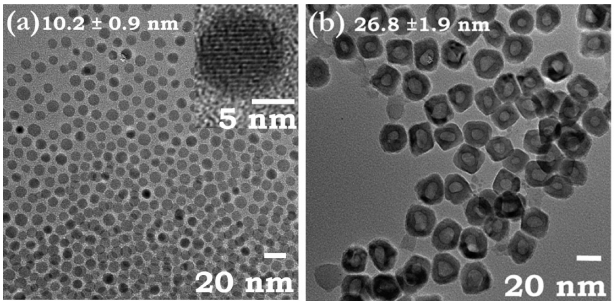

Figure 2. TEM images of (a) Ni_2P nanoparticles with solid morphology (inset: HRTEM indicating the high degree of crystallinity and the absence of voids) and (b) $Ni_{12}P_5$ nanoparticles with hollow morphology. An HRTEM image of a hollow $Ni_{12}P_5$ nanoparticle is given in Supporting Information Figure S5.

revealed a lower P:Ni ratio than for Ni_2P, consistent with formation of the more metal-rich phase (Figure S4b). The formation of hollow nanostructures can be attributed to the nanoscale Kirkendall effect, in which differences in ion diffusion rates results in voids, and were similar to those reported for Ni_2P[6,7] and mixed phase nickel phosphides[18] in the literature. To the best of our knowledge, this is the first report of low-polydispersity, phase-pure hollow $Ni_{12}P_5$ nanoparticles.

These observations clearly indicate that careful choice of reaction conditions cannot only enable control of the phase of the nanoparticles, but the size morphology as well. Increasing the P:Ni precursor ratio from 1.12 to 5.6 resulted in a decrease in the average size of the nanoparticles from 26.8 ± 1.9 nm ($Ni_{12}P_5$) to 10.2 ± 0.9 nm (Ni_2P). The decrease in size of the nanoparticles with increasing P:Ni precursor ratio in the system is consistent with previous observations made by Mèzailles and co-workers in their work on Ni nanoparticles and is attributed to the stabilization of the precursor nanoparticle surface by TOP, limiting particle growth.[23]

The variation in morphology between $Ni_{12}P_5$ and Ni_2P (hollow *vs* solid) can be attributed to the choice of precursor ratios chosen to stabilize these two different phases. These observations fall in line with the recent report on morphology control in Ni_xP_y nanoparticles by Tracy and co-workers.[18] They found that the P:Ni precursor ratios played an important role in determining the nature of the species formed at the precursor stage (220 °C), and the resultant morphology of the crystalline nickel phosphide formed at higher temperature (300 °C). Low P:Ni precursor ratios (1−3) resulted in the formation of crystalline Ni nanoparticles that subsequently transformed to hollow crystalline Ni_xP_y nanoparticles, high P:Ni precursor ratios (>9) resulted in the formation of Ni−P alloy nanoparticles that transformed to solid crystalline Ni_xP_y nanoparticles, and intermediate ratios produced a mixture of solid and hollow particles. In all cases, the samples of Tracy and co-workers were characterized to be mixtures of both $Ni_{12}P_5$ and Ni_2P phases.[18]

Effect of P:Ni Ratio on Precursor Crystallization and Composition—Step One of a Two-Pot Synthesis. The hypothesis regarding hollow and solid Ni_xP_y nanoparticle formation postulated by Tracy and co-workers[18] was tested under our synthetic conditions. The nature of the precursor nanoparticles formed at 200−230 °C was investigated as a function of the P:Ni precursor ratio. Precursor nanoparticles were prepared with P:Ni ratios in the range 0.28 to 5.6, aged for 60−90 min, and isolated at room temperature by precipitation with excess ethanol.

The PXRD pattern of precursor nanoparticles prepared with a ratio of 0.28 (prepared at 200 °C) was observed to be a direct match to the reference pattern of fcc-Ni (Figure 3); all three peaks corresponding to cubic phase Ni were observed. In addition, the nanoparticles were observed to respond strongly to a magnetic stir bar, consistent with the superparamagnetic nature of the Ni nanoparticles. A similar PXRD pattern is obtained for precursor nanoparticles

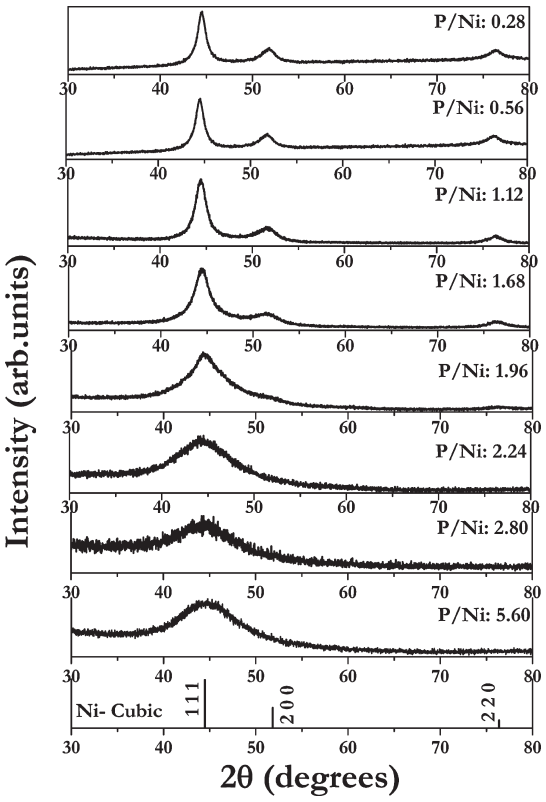

Figure 3. PXRD patterns of precursor nanoparticles (crystalline Ni and amorphous Ni_xP_y) prepared at 200−230 °C with varying P:Ni precursor ratios compared to the Ni reference pattern (PDF no. 87-0712).

prepared with P:Ni ratios of 0.56, 1.12, and 1.68 (prepared at 230 °C, Figure 3) and these nanoparticles also displayed a strong response to a magnet. TEM analyses were performed on precursor nanoparticles prepared with P:Ni of 0.28 and 1.12 and reveal the particles to be nearly spherical with an average size of 27.2 ± 2.4 and 21.1±1.4 nm, respectively (Figure 4a,b, Supporting Information, Figure S6a,b). EDS data on these samples are also consistent with Ni formation; only a small signal for P is observed, attributed to TOP ligands binding to the surface of Ni nanoparticles (Supporting Information, Figure S7).[5,23]

When the P:Ni was increased to 2.24 or higher, the PXRD patterns of the precursor nanoparticles indicated that the product was less crystalline (Figure 3). A broad peak around 44° 2θ, corresponding to the most intense peak of the fcc-Ni phase, was observed, while the two other characteristic Ni peaks were absent, suggesting lower crystallinity of the samples. The samples did not respond to a magnet at room temperature indicating a change in the magnetic characteristics of the material. TEM images acquired on nanoparticles prepared with P:Ni precursor ratios of 2.8 and 5.6 reveal the formation of spherical nanoparticles with an average size of 10.4 ± 0.8 and 9.6 ± 1.1 nm, respectively (Figure 4c,d, Supporting Information, Figure S6c,d). P:Ni ratios obtained from EDS analysis for both nanoparticles were found to be

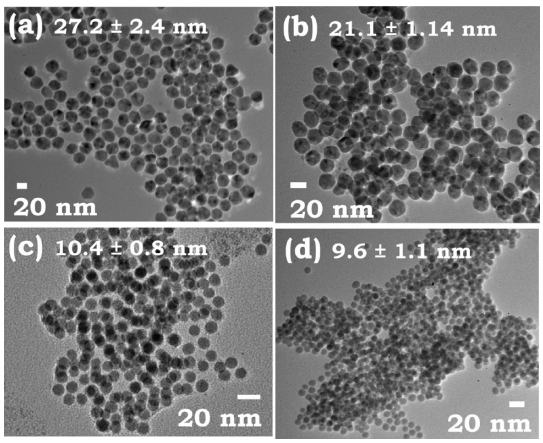

Figure 4. TEM images and average particle diameters of precursor nanoparticles (crystalline Ni and amorphous Ni_xP_y) prepared with varying P:Ni precursor ratios: (a) 0.28 (200 °C); (b) 1.12 (230 °C); (c) 2.8 (230 °C); and (d) 5.6 (230 °C). Histograms for the nanoparticles are given in Supporting Information Figure S6.

significantly higher than the crystalline Ni samples (Supporting Information, Figure S8). The high P content along with the broad feature in the PXRD pattern and unresponsiveness to an external magnet suggest the formation of an amorphous alloy of Ni−P. Note that amorphous Ni−P alloys with 20 wt % P are reported to lose their spontaneous magnetization;[24] likewise, there are no ferromagnetic crystalline nickel phosphides.[25] These results are qualitatively similar to those reported by Tracy and co-workers[18] for P:Ni ratios >9, but we see the transition from crystalline Ni to amorphous Ni_xP_y at considerably smaller ratios of P:Ni under our synthetic conditions. An intermediate P:Ni precursor ratio of 1.96 resulted in nanoparticles which exhibited all three peaks corresponding to cubic-Ni in the PXRD pattern, but the (111) reflection was found to be relatively broad in comparison to the (111) reflections of precursor nanoparticles prepared with lower P:Ni ratios (Figure 3). In addition, the sample was found to give a weak response to an external magnet, indicating that this stoichiometry reflects the crossover from magnetic Ni to nonmagnetic Ni_xP_y nanoparticles. These data are summarized in Supporting Information, Table S1. As already mentioned, the gradual decrease in the size of the nanoparticles with increasing P:Ni precursor ratio is attributed to the stabilization of the nanoparticle surface by TOP, which acts to limit growth *via* Ostwald ripening.[23]

Transformation of Crystalline Ni and Amorphous Ni_xP_y Nanoparticles to Hollow and Solid Ni_2P Nanoparticles—Step Two of a Two-Pot Synthesis Route. The isolated precursor nanoparticles were converted into crystalline Ni_2P by reaction with additional TOP in order to observe the effects of precursor composition on resultant morphology. To favor Ni_2P over $Ni_{12}P_5$, we used a higher conversion temperature (350 °C) relative to Tracy and co-workers (300 °C) and simultaneously employed longer reaction times (3−4 h) and large concentrations of TOP (>10 times the estimated

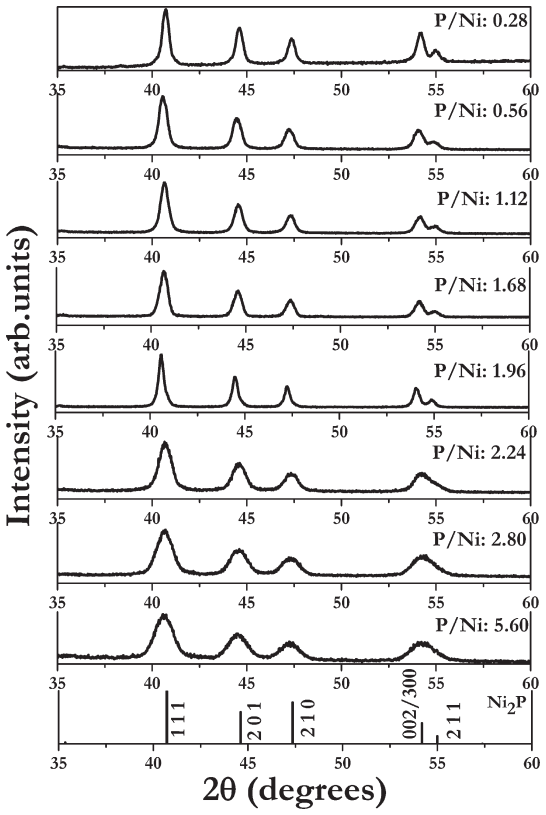

Figure 5. PXRD patterns of the final products obtained by the reaction of the various precursor nanoparticles with TOP at 350 °C for 3−4 h compared to the Ni_2P reference pattern (PDF no. 74-1385). The P/Ni ratios correspond to those used to form the precursor nanoparticles.

moles of Ni in the reaction). Approximately 50 mg of each of the precursor nanoparticle samples depicted in Figure 3 were combined with 10.0 mL of octyl ether and 2.0 mL of oleylamine and subsequently reacted with 11.2 mmol of TOP at 350 °C for about 3−4 h. The isolated products showed no response to the stir bar, suggesting they are free of crystalline Ni impurities. Products were characterized by PXRD and the patterns indicated that all precursor nanoparticles were completely converted into crystalline phase-pure samples of Ni_2P (Figure 5). Size differences are apparent between Ni_2P nanoparticles obtained from crystalline Ni nanoparticles and those from the amorphous Ni_xP_y nanoparticles. The PXRD peaks were all broader, and peaks corresponding to (002/300) and (211) reflections were found to merge together, for the Ni_2P nanoparticles obtained from amorphous Ni_xP_y nanoparticles, whereas the reflections can be identified discretely for Ni_2P nanoparticles obtained from crystalline Ni nanoparticles. Crystallite size calculations made by applying the Scherrer equation to (111) reflections of Ni_2P nanoparticles substantiate the qualitative observations made from the PXRD patterns (Supporting Information, Table S1). Overall, Ni_2P obtained from the crystalline Ni precursor nanoparticles are comparatively larger in size relative to products obtained from amorphous Ni_xP_y nanoparticles.

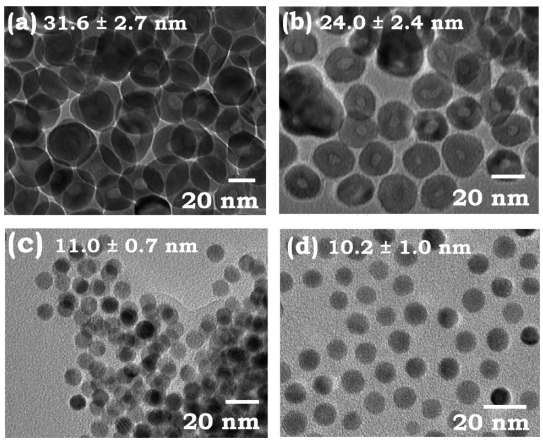

Figure 6. TEM images and average particle diameters of Ni_2P nanoparticles obtained from reaction of additional TOP with different precursor nanoparticles prepared with varying P:Ni ratios: (a) 0.28; (b) 1.12; (c) 2.8; and (d) 5.6. Histograms for the nanoparticles are given in Supporting Information Figure S9.

TEM analyses (Figure 6) of Ni_2P nanoparticles are in rough agreement with the PXRD crystallite size calculations as shown in Supporting Information, Table S1. However, crystallite size calculations significantly underestimate sizes for hollow nanoparticles due to the presence of the void. Ni_2P nanoparticles obtained from crystalline Ni nanoparticles depicted in Figure 4 panels a (27.2 ± 2.4 nm) and b (21.1 ± 1.4 nm) were found to be composed of hollow structures with an average particle size 31.6 ± 2.7 and 24.0 ± 2.4 nm, respectively (Figure 6a,b, Supporting Information, Figure S9a,b). The *ca.* 15% increase in size during transformation to Ni_2P is expected due to the incorporation of phosphorus and the formation of hollow voids within the particles. The formation of hollow structures can be attributed to the nanoscale Kirkendall effect, previously observed in nickel phosphides.[6,7] This effect arises from a diffusion couple between Ni and P wherein Ni migration outward is faster than P migration inward, leading to void formation. On the other hand, the Ni_2P nanoparticles obtained from amorphous Ni_xP_y nanoparticles depicted in Figure 4 panels c (10.4 ± 0.8 nm) and d (9.6 ± 1.1 nm) resulted in solid spherical nanoparticles of size 11.0 ± 0.7 and 10.2 ± 1.0 nm, respectively (Figure 6c,d, Supporting Information, Figure S9c,d). Presumably, the presence of phosphorus in the particles, and possibly their smaller size, precludes significant migration rate differences, at least to an extent that would produce voids. In contrast to the hollow structure formation, the size increase due to P incorporation in the lattice is considerably smaller (5−6%), as expected for a solid phase.

These results clearly indicate that the morphology and size of the final product is dictated by the initial P:Ni precursor ratio chosen for a particular synthesis, either due to variation in crystallinity/composition of the precursor particles or to the size difference (crystalline Ni

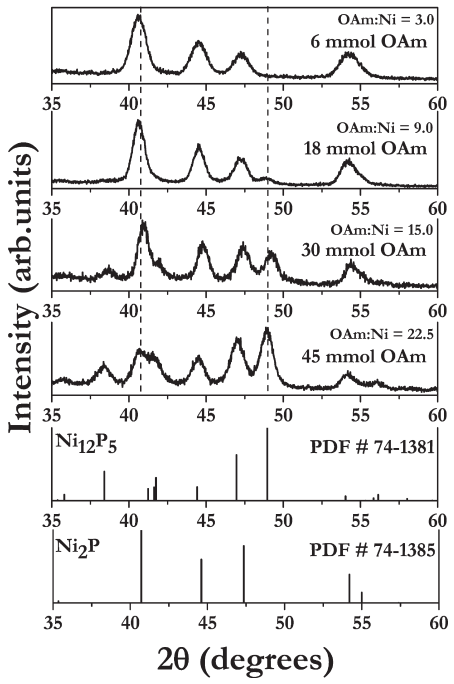

Figure 7. PXRD patterns of final products prepared with varying oleylamine quantity compared to reference patterns of $Ni_{12}P_5$ and Ni_2P (P:Ni = 5.6, 2 mmol Ni, 11.2 mmol TOP, 3 h, 350 °C). The dashed lines indicate the most intense peaks corresponding to Ni_2P and $Ni_{12}P_5$.

precursor particles have diameters 2−3 times larger than the amorphous alloy particles). These results also show that conditions exist whereby a single phase product (Ni_2P) can be produced with hollow and solid morphologies. The Ni_2P phase was achieved by carrying out the conversion reactions for longer times (3−4 h) with larger concentrations of TOP (>10 times that of Ni) at higher temperatures (350 °C) which ensured adequate availability of reactive phosphorus for the formation of the more P-rich phase among the accessible phases in this synthesis (Ni_2P over $Ni_{12}P_5$).

Effect of Oleylamine: Generation of Solid $Ni_{12}P_5$ Nanoparticles Using a One-Pot Synthesis Route. The preparation of solid $Ni_{12}P_5$ nanoparticles proved to be a challenge as a P:Ni precursor ratio of 2.8 or higher is needed to generate solid nanoparticles, but such high ratios favor formation of the more P-rich phase (Ni_2P) during conversion to the phosphide phase. To favor a more metal-rich phase, we explored the role of oleylamine as a modifier in the reaction.

A series of reactions by the one-pot route in which Ni nanoparticles are formed at 230 °C, but not isolated, and then transformed to nickel phosphides, was performed wherein the quantity of oleylamine was varied systematically while keeping all other reaction parameters constant. The reactions were carried out under conditions optimized for the solid Ni_2P nanoparticle synthesis (P:Ni = 5.6, 3 h, 350 °C). The ratio of oleylamine/Ni used in the reaction was varied from 3 to 22.5 and the PXRD patterns (Figure 7) of the isolated final products clearly indicated that higher amounts of oleylamine favors formation of the metal-rich phase, $Ni_{12}P_5$. Specifically, the most intense peak corresponding to $Ni_{12}P_5$ was found to grow gradually with increasing oleylamine quantity and $Ni_{12}P_5$ was found to be the major product when the oleylamine/Ni ratio was 22.5. The exact mechanism by which oleylamine tends to favor the metal-rich phase ($Ni_{12}P_5$) under conditions more suitable for the formation of Ni_2P is not known. However, amines are purported to play the role of reducing agent in metal nanoparticle syntheses,[23,26] and thus the presence of excess amine could promote the stabilization of the more reduced phase ($Ni_{12}P_5$). Alternatively, excess amine could also displace the phosphine ligands from the precursor nanocrystal surface and create a lack of reactive phosphorus, thereby resulting in a metal-rich phase. A similar observation has been reported in the literature by Hyeon and coworkers wherein they observed that the use of oleylamine favored the formation of metal-rich Fe_2P under conditions typically employed for FeP.[4,27]

The positive influence of the excess amine in stabilizing $Ni_{12}P_5$, even under conditions that favor the formation of Ni_2P, provided insight for optimizing conditions for the preparation of $Ni_{12}P_5$ nanoparticles with a solid morphology. A solid morphology requires a relatively high P:Ni ratio (favoring Ni_2P) but this may be offset by use of excess amine to promote the stabilization of a metal-rich phase ($Ni_{12}P_5$). Accordingly, we carried out a reaction series by a one-pot route wherein the P:Ni precursor ratio was gradually varied from 1.12 to 5.6. All four reactions were carried out under identical conditions and utilized a high concentration of oleylamine (60 mmol oleylamine, 4 mmol Ni, 1 h, 350 °C). As expected, the addition of excess oleylamine was observed to stabilize the metal-rich phase $Ni_{12}P_5$ (Figure 8). All four samples were observed to be phase-pure; peaks corresponding to the Ni_2P phase are not observed.

TEM analyses of the $Ni_{12}P_5$ nanoparticles prepared with a P:Ni precursor ratio of 1.12 revealed the sample to be composed of hollow nanoparticles (Figure 9a, Supporting Information, Figure S10a) with an average size of 25.3 ± 2.5 nm. A gradual increase in P:Ni precursor ratio to 5.6 results in the transformation of hollow nanoparticles into solid spherical nanoparticles while simultaneously resulting in smaller nanoparticles (Figure 9b,c,d, Supporting Information, Figure S10b,c, d) consistent with the observation for Ni_2P. EDS analyses carried out on all nanoparticles are consistent with the stabilization of the $Ni_{12}P_5$ phase (Supporting Information, Figure S11), demonstrating a similar ratio to the ideal P:Ni ratio for $Ni_{12}P_5$ (0.42).

To demonstrate that the use of an excess of amine is essential for the generation of solid $Ni_{12}P_5$, a set of control reactions (positive and negative) by one-pot route was carried out for a P:Ni precursor ratio of 5.6.

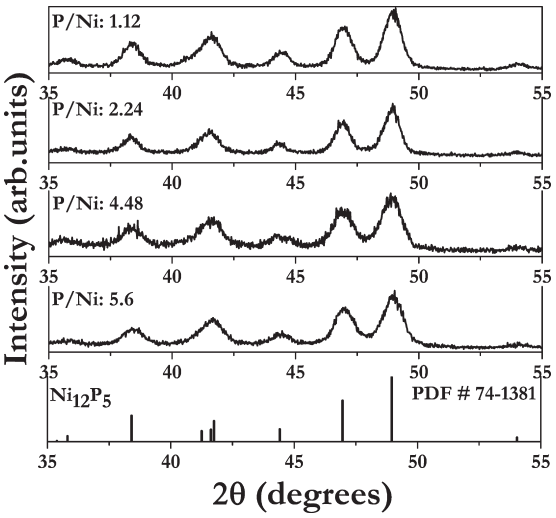

Figure 8. PXRD patterns of $Ni_{12}P_5$ nanoparticles compared to reference pattern (PDF no. 74-1381), prepared with varied P:Ni precursor ratios (60 mmol oleylamine, 4 mmol Ni, 1 h, 350 °C).

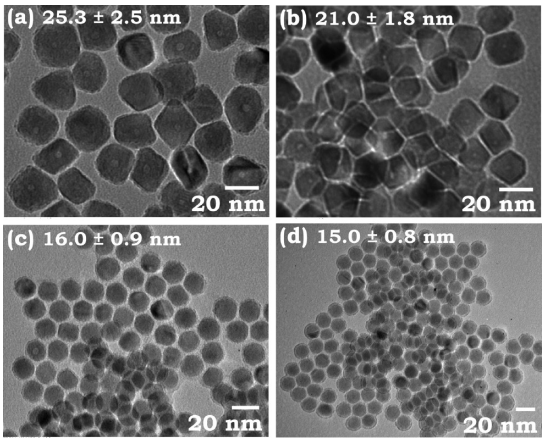

Figure 9. TEM images and average particle diameters of $Ni_{12}P_5$ nanoparticles prepared with varied precursor P:Ni ratios: (a)1.12, (b) 2.24, (c) 4.48, and (d) 5.6. The corresponding histograms are available in Supporting Information Figure S10.

The PXRD patterns and TEM images of the reaction products are shown in Figure 10. As expected, all the nanoparticles were observed to possess a solid morphology as dictated by the P:Ni precursor ratio (5.6), and when the reaction was carried out without the additional quantity of oleylamine, the product was characterized to be Ni_2P (Figure 10a). To discount the effect of dilution that occurs on addition of excess oleylamine to the reaction, a control was run in which the system was diluted by an equivalent volume (16.0 mL) of octyl ether (noncoordinating solvent) in lieu of amine. The product of the reaction was again determined to be Ni_2P (Figure 10b). In the last control reaction, the excess oleylamine was replaced by an equivalent quantity (in moles) of octadecylamine (Figure 10c). This time, the product of the reaction was characterized to be $Ni_{12}P_5$. These results confirm the requirement of excess amine to promote the stabilization of solid $Ni_{12}P_5$ nanoparticles.

It should also be noted that the addition of excess oleylamine also impacts the size of the voids in hollow structures. A size comparison made between the hollow structures of $Ni_{12}P_5$ nanoparticles prepared with different oleylamine quantities indicates that higher oleylamine quantities results in smaller voids (Supporting Information, Figure S12) for product particles that are of similar size. The smaller voids likely result from a decrease in the quantity of bound TOP at the particle surface due to competition with oleylamine. Less TOP means less activated P at the particle surface, potentially altering the Ni−P diffusion couple such that diffusion of Ni outward is slowed just as P diffusion inward is slowed. Thus, oleylamine countermands the tendency toward hollow structure formation, at the same time favoring the more metal-rich phase.

Interdependency of Synthetic Levers: Temperature, Heating Time, and TOP Quantity. Temperature, heating time and TOP quantity all play major roles in controlling the amount of phosphorus available to react with the nickel species in solution. Thus, a decrease in one factor can be compensated by increasing another factor. For example, a small decrease in reaction temperature can be offset by either increasing the reaction time or TOP quantity. The interdependency of these "synthetic levers" is qualitatively displayed in Scheme 2, and explains why mixed phases are the "norm", and phase-pure samples require some finesse. Size and morphology are controlled by varying the P:Ni ratio in the synthesis of the precursor particles at 200−230 °C, with large, hollow particles forming at low P:Ni and small, solid particles forming at high P:Ni. Of course, the P:Ni ratio also impacts the phase at the crystallization temperature (300−350 °C), with metal-rich $Ni_{12}P_5$ generated at low P:Ni and Ni_2P at high P:Ni. However, the product phase formed can be decoupled from the initial precursor ratio (which dictates whether crystalline Ni or amorphous Ni_xP_y precursor nanoparticles forms, and consequently, hollow or solid particles) by addition of more TOP at the crystallization temperature. This enables formation of hollow particles (favored by low P:Ni) of Ni_2P (favored by high P:Ni). Increasing temperature and heating time also favor formation of the more P-rich Ni_2P phase, by generating more reactive P and providing sufficient time for conversion to the thermodynamic product. On the other hand, generating the metal-rich $Ni_{12}P_5$ phase under high P:Ni precursor ratios that favor solid particle formation can be achieved by the addition of oleylamine, which appears to function as a reducing agent or limits phosphorus inclusion by competitive binding *versus* TOP. Oleylamine also can act to "tune" the size of the voids in particles formed at low P:Ni ratios, enabling

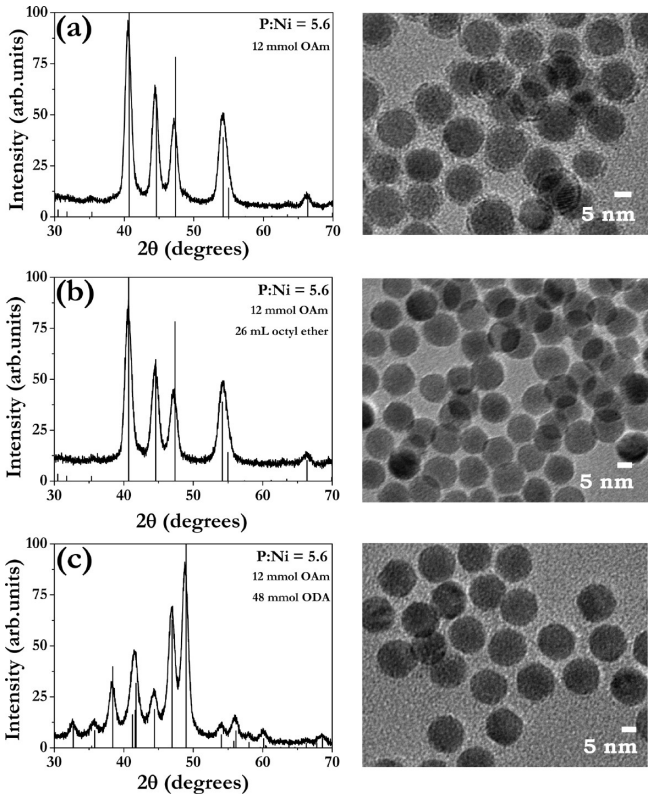

Figure 10. PXRD patterns and TEM images of the final product of the control reactions carried out to prove the effect of excess amine on the $Ni_{12}P_5$ solid nanoparticle synthesis: (a) without excess oleylamine (OAm), (b) with excess octyl ether (solvent) in lieu of OAm, and (c) with excess octadecylamine in lieu of OAm.

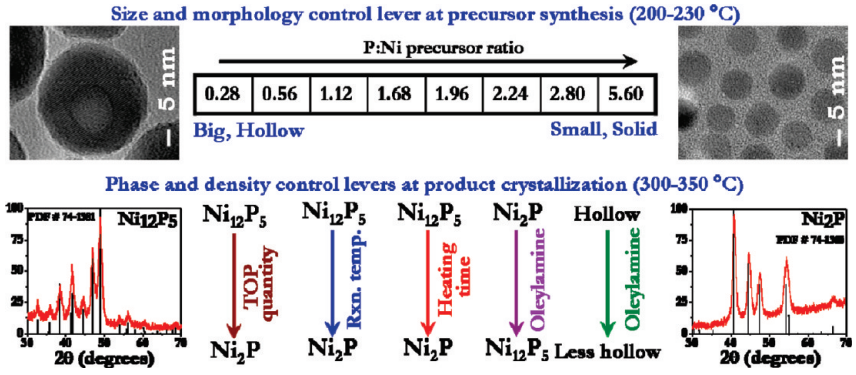

Scheme 2. Illustration of the roles played by various synthetic levers in controlling the size, morphology, and phase in nickel phosphide nanoparticles.

$Ni_{12}P_5$ particles with a range of void sizes, but similar overall particle sizes, to be produced.

With respect to general applicability of the concepts here toward other Ni−P nanoparticle phases, we note that only a few reports are available on the nanoscale preparation of P-rich nickel phosphides[28−30] and P-rich Ni_xP_y nanoparticles are yet to be prepared *via* the metal−nanoparticle conversion method. We believe that the P-rich phases such as Ni_5P_4 and NiP_2 can be generated by working under conditions that will help generate higher amounts of reactive phosphorus in the system. These include higher reaction temperatures (>350 °C), high P:Ni precursor ratio, and cannulation of hot metal nanoparticles (>200 °C) into preheated TOP (350 °C).

CONCLUSION

Reaction parameters have been utilized as levers to tune phase, size, and morphology, enabling phase-pure samples of $Ni_{12}P_5$ and Ni_2P to be prepared in both solid and hollow morphologies. The P:Ni precursor ratio has been identified as the primary synthetic lever operating at the precursor particle formation temperature, controlling morphology. At the nickel phosphide crystallization temperature, addition of TOP, reaction time, and temperature played key roles in stabilizing

the final phase of the product, enabling formation of hollow particles of $Ni_{12}P_5$ and Ni_2P and solid particles of Ni_2P. Excess oleylamine stabilized the more reduced phase, $Ni_{12}P_5$, offsetting the effects of a high P:Ni ratio and enabling this phase to be realized in solid morphology, as well as reducing the void size in hollow structures. The exquisite control demonstrated in the synthesis is expected to enable phase, morphology, and size-dependent hydrodesulfurization activities of nanoscale Ni−P to be systematically probed for the first time, a study that is presently underway. Moreover, the general concepts developed in the course of this Ni−P investigation should be applicable to other nanoparticle conversion reactions, decreasing the time and effort needed to produce targeted phases with controlled stoichiometry, morphology, and size.

METHODS

Chemicals. Nickel acetylacetonate ($Ni(acac)_2$, 95%), was purchased from Alfa Aesar. Tri-*n*-octylphosphine (TOP, 97%) was purchased from STREM and was stored under argon in a glovebox. *n*-Octyl ether was purchased from TCI America. Oleylamine (C18 content 80−90%) and octadecylamine (tech. 90%) were purchased from ACROS. The solvents chloroform and ethanol (200 proof) were purchased from Fisher Scientific and Decon Laboratories, Inc., respectively. All chemicals were used as received.

Synthesis. All reactions were carried out in argon atmosphere using standard Schlenk line techniques. Two different approaches were followed to prepare nickel phosphide nanoparticles (Scheme 1): (i) a one-pot strategy involving $Ni(acac)_2$ and TOP in the synthesis of precursor nanoparticles at 230 °C and subsequent conversion to crystalline phosphide phase at 300−350 °C; and (ii) a two-pot strategy in which the precursor nanoparticles were isolated after the reaction at 200−230 °C, then subsequently redispersed in octyl ether and oleylamine and reacted with TOP, the phosphorus precursor, at 350 °C.

In a typical one-pot synthesis, both Ni and P precursors were combined with 10.0 mL of octyl ether (solvent) and 2.0−4.0 mL (~6−12 mmol) oleylamine (surfactant) in a Schlenk flask fitted with a reflux condenser vented by an oil bubbler and degassed at 100 °C under partial vacuum. Heat was introduced *via* a heating mantle, and the temperature was maintained using a digital temperature controller with the thermocouple placed within the mantle, near the bottom of the flask. The system was then heated to 230 °C under Ar, where it was maintained for 60−90 min yielding a black solution. The temperature was then raised to 300−350 °C for 1−3 h, depending on the phase desired. The nanoparticles were isolated after returning the system to room temperature (RT) by the addition of 20−30 mL ethanol followed by centrifugation. Isolated nanoparticles were then dispersed in 1−2 mL of chloroform with sonication and reprecipitated with excess ethanol. The process was carried out twice, and the washed product was dried under vacuum to yield a free-flowing powder.

In the two-pot strategy, precursor nanoparticles were synthesized at 200−230 °C as described above and isolated at RT by precipitation with excess ethanol and centrifugation. The isolated precursor nanoparticles were then dispersed in 1−2 mL of chloroform and reprecipitated with excess ethanol. Subsequently, a known quantity (50 mg) of the isolated nanoparticles was combined with octyl ether (10.0 mL) and oleylamine (2.0 mL, 6 mmol). The system was degassed under vacuum at 100 °C and was raised to 300 °C under Ar. After 10−15 min at 300 °C, 10.0 mL of TOP was injected into the system, followed by a raise in temperature to 350 °C where it was maintained for 3−4 h. Isolation of the final product was carried out as described for the one-pot synthesis.

Reactions were also carried out in which the oleylamine quantity was systematically varied in the range 6.0−45.0 mmol, with a P:Ni precursor ratio of 5.6. The conversion reactions were carried out at 350 °C for 3−4 h after the preparation of precursor nanoparticles at 230 °C (90 min). On the basis of these data, solid $Ni_{12}P_5$ nanoparticles were synthesized by the one-pot route by choosing a high ratio of oleylamine:Ni (4 mmol Ni, 60 mmol oleylamine) for the P:Ni precursor ratio of 5.6, and a 1 h reaction time. The precursor nanoparticles were made at 230 °C, and the subsequent conversion was carried out for 1 h at 350 °C.

Characterization Techniques. Powder X-ray diffraction (PXRD) was carried out on a Rigaku diffractometer RU200B with a Cu Kα rotating anode. Samples were deposited onto a zero background quartz holder with a thin layer of grease. Phase was assigned by comparison to the powder diffraction files (PDFs) of the International Center of Diffraction Data (ICDD) using Jade 5.0 software.

Transmission electron microscopy (TEM) and semiquantitative energy dispersive spectroscopy (EDS) were performed using a JEOL FasTEM 2010 electron microscope operated at a voltage of 200 kV and a beam current of 107−108 μA with a coupled EDS detector (EDAX Inc.). The images were captured using Amtv600 software provided by the Advanced Microscopy Techniques Corporation. Samples for TEM analysis were prepared by depositing a drop of chloroform nanoparticle dispersion onto a carbon-coated 200 mesh Cu grid, followed by air-drying.

Acknowledgment. We thank Y. Liu and M. J. Heeg for assistance with electron microscopy and powder X-ray diffraction, respectively. This work was supported by the National Science Foundation (DMR-0094273 and DMR-0701161). Electron microscopy was acquired on a JEOL 2010 FasTEM purchased under NSF Grant DMR-0216084.

Supporting Information Available: Powder X-ray diffraction data for time-dependent reactions at two different temperatures; particle size histograms and EDS data for precursor and product nanoparticles; high resolution TEM data for hollow $Ni_{12}P_5$ particles; table depicting the effect of precursor P:Ni ratio on the precursor nanoparticle and the final product (Ni_2P) characteristics; void sizes for hollow $Ni_{12}P_5$ particles as a function of oleylamine quantity. This material is available free of charge *via* the Internet at http://pubs.acs.org.

REFERENCES AND NOTES

1. Wang, X.; Clark, P.; Oyama, T. S. Synthesis, Characterization, and Hydrotreating Activity of Several Iron Group Transition Metal Phosphides. *J. Catal.* **2002,** *208*, 321–331.
2. Oyama, T., S. Novel Catalysts for Advanced Hydroprocessing: Transition Metal Phosphides. *J. Catal.* **2003,** *216*, 343–352.
3. Oyama, T., S.; Gott, T.; Zhao, H.; Lee, Y.-K. Transition Metal Phosphide Hydroprocessing Catalysts: A Review. *Catal. Today* **2009,** *143*, 94–107.
4. Park, J.; Koo, B.; Yoon, K., Y; Hwang, Y.; Kang, M.; Park, J.-G.; Hyeon, T. Generalized Synthesis of Metal Phosphide Nanorods *via* Thermal Decomposition of Continuously Delivered Metal−Phosphine Complexes Using a Syringe Pump. *J. Am. Chem. Soc.* **2005,** *127*, 8433–8440.
5. Senevirathne, K.; Burns, A. W.; Bussell, M. E.; Brock, S. L. Synthesis and Characterization of Discrete Nickel Phosphide Nanoparticles: Effect of Surface Ligation Chemistry on Catalytic Hydrodesulfurization of Thiophene. *Adv. Funct. Mater.* **2007,** *17*, 3933–3939.
6. Chiang, R.-K.; Chiang, R.-T. Formation of Hollow Ni_2P Nanoparticles Based on the Nanoscale Kirkendall Effect. *Inorg. Chem.* **2007,** *46*, 369–371.

7. Henkes, A. E.; Vasquez, Y.; Schaak, R. E. Converting Metals into Phosphides: A General Strategy for the Synthesis of Metal Phosphide Nanocrystals. *J. Am. Chem. Soc.* **2007,** *129*, 1896–1897.
8. Maneeprakorn, W.; Nguyen, C. Q.; Malik, M. A.; O'Brien, P.; Raftery, J. Synthesis of the Nickel Selenophosphinates $[Ni(Se_2PR_2)_2]$ (R = Pr, Bu, and Ph) and Their Use as Single Source Precursors for the Deposition of Nickel Phosphide or Nickel Selenide Nanoparticles. *Dalton Trans.* **2009,** 2103–2108.
9. Sawhill, S. J.; Phillips, D. C.; Bussell, M. E. Thiophene Hydrodesulfurization Over Supported Nickel Phosphide Catalysts. *J. Catal.* **2003,** *215*, 208–219.
10. Sawhill, S. J.; Layman, K. A.; Van Wyk, D. R.; Engelhard, M. H.; Wang, C.; Bussell, M. E. Thiophene Hydrodesulfurization over Nickel Phosphide Catalysts: Effect of the Precursor Composition and Support. *J. Catal.* **2005,** *231*, 300–313.
11. Yang, S.; Prins, R. New Synthesis Method for Nickel Phosphide Hydrotreating Catalysts. *Chem. Commun.* **2005,** 4178–4180.
12. Panneerselvam, A.; Malik, M., A; Afzaal, M.; O'Brien, P.; Helliwell, M. The Chemical Vapor Deposition of Nickel Phosphide or Selenide Thin Films from a Single Precursor. *J. Am. Chem. Soc.* **2008,** *130*, 2420–2421.
13. Liu, S.; Liu, X.; Xu, L.; Qian, Y.; Ma, X. Controlled Synthesis and Characterization of Nickel Phosphide Nanocrystal. *J. Cryst. Growth* **2007,** *304*, 430–434.
14. Hu, X.; Yu, J. C. High-Yield Synthesis of Nickel and Nickel Phosphide Nanowires *via* Microwave-Assisted Processes. *Chem. Mater.* **2008,** *20*, 6743–6749.
15. Muthuswamy, E.; Brock, S., L. Oxidation Does Not (Always) Kill Reactivity of Transition Metals: Solution-Phase Conversion of Nanoscale Transition Metal Oxides to Phosphides and Sulfides. *J. Am. Chem. Soc.* **2010,** *132*, 15849–15851.
16. Henkes, A. E.; Schaak, R. E. Trioctylphosphine: A General Phosphorus Source for the Low-Temperature Conversion of Metals into Metal Phosphides. *Chem. Mater.* **2007,** *19*, 4234–4232.
17. Zheng, X.; Yuan, S.; Tian, Z.; Yin, S.; He, J.; Liu, K.; Liu, L. One-Pot Synthesis of Hollow Nickel Phosphide Nanoparticles with Tunable Void Sizes Using Triphenylphosphine. *Mater. Lett.* **2009,** *63*, 2283–2285.
18. Wang, J.; Johnston-Peck, A., C; Tracy, J. B. Nickel Phosphide Nanoparticles with Hollow, Solid, and Amorphous Structures. *Chem. Mater.* **2009,** *21*, 4462–4467.
19. Muthuswamy, E.; Kharel, P., R; Lawes, G.; Brock, S., L. Control of Phase in Phosphide Nanoparticles Produced by Metal Nanoparticle Transformation: Fe_2P and FeP. *ACS Nano* **2009,** *3*, 2383–2393.
20. Kim, H.; Chae, Y.; Lee, D. H.; Kim, M.; Huh, J.; Kim, Y.; Kim, H.; Kim, H. J.; Kim, S. O.; Baik, H.; *et al*. Palladium Nanoparticle Catalyzed Conversion of Iron Nanoparticles into Diameter- and Length-Controlled Fe_2P Nanorods. *Angew. Chem., Int. Ed.* **2010,** *49*, 5712–5716.
21. Ni, Y.; Tao, A.; Hu, G.; Cao, X.; Wei, X.; Yang, Z. Synthesis, Characterization and Properties of Hollow Nickel Phosphide Nanospheres. *Nanotechnology* **2006,** *17*, 5013–5018.
22. Li, J.; Ni, Y.; Liao, K.; Hong, J. Hydrothermal Synthesis of $Ni_{12}P_5$ Hollow Microspheres, Characterization and Photocatalytic Degradation Property. *J. Colloid Interface Sci.* **2009,** *332*, 231–236.
23. Carenco, S.; Boissere, C.; Nicole, L.; Sanchez, C.; Le Floch, P.; Mezailles, N. Controlled Design of Size-Tunable Monodisperse Nickel Nanoparticles. *Chem. Mater.* **2010,** *22*, 1340–1349.
24. Wachtel, E.; Willmann, N.; Bahle, J.; Bakonyi, I.; Lovas, A.; Liebermann, H. H. Magnetic Properties of Amorphous and Liquid Ni−P Alloys Around 20 at. % P. *J. Phys. Colloques* **1988,** *49*, C8–1277-C8−1278.
25. Hulliger, F. Crystal Chemistry of the Chalcogenides and Pnictides of the Transition Elements. *Struct. Bonding (Berlin)* **1968,** *4*, 83–229.
26. Hou, Y.-L.; Gao, S. Solvothermal Reduction Synthesis and Magnetic Properties of Polymer Protected Iron and Nickel Nanocrystals. *J. Alloys Compd.* **2004,** *365*, 112–115.
27. Park, J.; Koo, B.; Hwang, Y.; Bae, C.; An, K.; Park, J.-G.; Park, H., M; Hyeon, T. Novel Synthesis of Magnetic Fe_2P Nanorods from Thermal Decomposition of Continuously Delivered Precursors Using a Syringe Pump. *Angew. Chem., Int. Ed.* **2004,** *43*, 2282–2285.
28. Barry, B. M.; Gillan, E. G. Low-Temperature Solvothermal Synthesis of Phosphorus-Rich Transition-Metal Phosphides. *Chem. Mater.* **2008,** *20*, 2618–2620.
29. Barry, B. M.; Gillan, E. G. A General and Flexible Synthesis of Transition-Metal Polyphosphides *via* PCl_3 Elimination. *Chem. Mater.* **2009,** *21*, 4454–4461.
30. Wang, J.; Yang, Q.; Zhang, Z.; Sun, S. Phase-Controlled Synthesis of Transition-Metal Phosphide Nanowires by Ullmann-Type Reactions. *Chem.—Eur. J.* **2010,** *16*, 7916–7924.